RSC Advances

PAPER

View Article Online
View Journal | View Issue

Cite this: *RSC Adv.*, 2017, **7**, 50889

Quantitative detection of H_2S and CS_2 mixed gases based on UV absorption spectrometry

Xiaoxing Zhang, *[a] Zhaolun Cui,[a] Zheng Cheng,[b] Yalong Li[a] and Hai Xiao[c]

Received 7th September 2017
Accepted 23rd October 2017

DOI: 10.1039/c7ra09983e

rsc.li/rsc-advances

H_2S and CS_2 are the decomposition components of insulating gas SF_6. The detection of these two gases is significant for the online monitoring and fault diagnosis of SF_6 electrical equipment. In this study, an ultraviolet (UV) differential optical absorption spectrometry (UV-DOAS) platform is established for detecting the concentration of H_2S and CS_2 mixed gases. Based on the platform, we obtained the UV absorption spectra of the two gases. The linear relationship between each gas absorption spectra and the concentration was established by wavelet processing and frequency analysis. The interference between the two gases in the UV spectrum region was studied. H_2S at different concentrations had little effect on the UV absorption spectra of CS_2. The linearity (R^2) of CS_2 inversion formula was 0.9997. CS_2 above 50 ppb produces a great interference on H_2S concentration detection. CS_2 concentration has a linear relationship with the H_2S concentration inversion; hence, the H_2S correction formula with CS_2 concentration as the variable is proposed. With the correction formula, the linearity (R^2) of H_2S inversion formula reaches 0.9994 in mixed gas detection, which can meet the H_2S and CS_2 mixed gases quantitative detection.

1 Introduction

Sulfur hexafluoride (SF_6) has good electrical properties and excellent arc suppression performance. As an insulating gas, SF_6 is widely used in a variety of high-voltage electrical equipment.[1,2] In the SF_6 insulation equipment, partial discharge (PD), partial overthermal faults (POF), and other failures may cause the decomposition of SF_6; this finding may result in CS_2, SO_2, H_2S, SOF_2, and SO_2F_2 decomposition components. These decomposition components on one hand will exacerbate the equipment faults, on the other hand may cause harm to the safety of personnel. Therefore, SF6 decomposition components and the monitoring of insulation faults, such as PD, must be diagnosed.[3–5]

H_2S occurs mainly in the SF_6 overheating decomposition like PD and POF with trace moisture involved. SF_6 decomposes and generates S^{2-} after the collision, H_2O breaks and generates H^+. S^{2-} and H^+ eventually combine to generate H_2S.[6] The chemical formula of the reaction mechanism is described as follows:

$$SF_6 + 2e \rightarrow S^{2-} + 6F \quad (1)$$

$$S^{2-} + 2H^+ \rightarrow H_2S \quad (2)$$

In relevant studies, CS_2 occurs in PD and POF failures when the molecular structure of epoxy insulator deteriorates in relatively high temperature. Some active pieces like CH_2, CH and C will be generated and react with SF_6 or its decompositions.[7] Generate path of CS2 is showed in Fig. 1.

Among them, C atoms are derived from organic insulating materials and stainless steel, and S atoms are derived from SF_6. Generation of S atoms requires SF_6 to break six S–F bonds, which correspond to a higher energy; hence, CS_2 can be detected at higher temperatures. Known from the Arrhenius law[8] in the chemical reaction kinetics, the chemical reaction rate is exponentially related to the reaction temperature. When the local overheat temperature is low, the CS_2 generation reaction is slow; when the local overheat temperature is high, CS_2 generation reaction abruptly accelerates. CS_2 is an important characteristic component to judge the existence of solid insulation

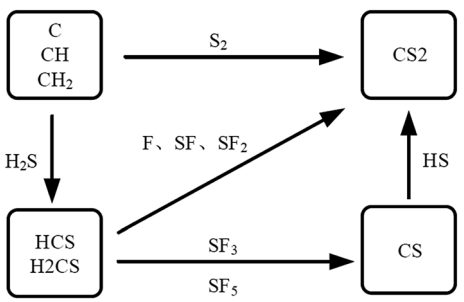

Fig. 1 Generate path of CS_2.

[a]School of Electrical Engineering, Wuhan University, Wuhan 430072, China. E-mail: xiaoxing.zhang@outlook.com
[b]State Grid Electric Power Company of Chongqing, Yongchuan, 402160, China
[c]Department of Electrical and Computer Engineering, Center for Optical Material Science and Engineering Technologies (COMSET), Clemson University, Clemson, South Carolina 29634, USA

defects. CS_2 detection is of great significance to the fault diagnosis of SF_6 insulation equipment.

At present, the detection of SF_6 characteristic decomposition components is achieved by two main methods: chemical detection methods and optical detection methods. Chemical gas detection methods include gas sensor method, detection tube method, and gas chromatography method;[9,10] optical methods include infrared Fourier transform spectroscopy, photoacoustic spectroscopy, and ultraviolet (UV) absorption spectroscopy. In comparison with the optical detection method, the chemical detection method has the characteristics of long detection time and high detection precision. Long detection time makes it not suitable for online monitoring. The infrared absorption spectrum can realize online monitoring. However, the infrared absorption characteristic peaks of SF_6 gas and various component gases are very close, and the overlapping of characteristic peaks easily occurs, which limits the detection accuracy. Photoelectric spectrum method has a high sensitivity but is susceptible to ambient temperature, pressure, and external noise.[11–13] The above methods have limitations in the online monitoring of the SF_6 characteristic decomposition component.

The external electrons in the molecules are excited by photons in different energy levels. The number of electron layers of different molecules and the energy levels of each layer are different; hence, difference in UV absorption spectra of different molecules is observed. One way to quantitatively study of a unknown gas can be realized by analyzing the peak position and peak of the absorption spectrum. UV differential optical absorption spectrometry (UV-DOAS), by fitting the slow absorption part of the original absorption spectrum and subtracting it, can effectively eliminate the influence of spectral absorption caused by Rayleigh scattering and Mie scattering on the gas concentration measurement and has strong anti-interference ability.[14,15]

H_2S and CS_2, as the important decomposition products of SF6 in the PD and POF insulation failure under, have absorption peaks in the UV spectrum region. Among them, H_2S absorption peaks distribute in 180–230 nm, and CS_2 absorption peak distribute in 190–210 nm; an overlap between the two gases' absorption peaks is found.

In 1963, Kleman *et al.* studied the absorption properties of CS_2 at 190–210 nm. CS_2 spectrum in the range of 285–340 nm was obtained by Ahmed and Kumr.[10] Due to the weak absorption at 285–340 nm band, when the light path is short or the low UV lamp power is low, the absorption cannot be measured in the band; hence, this study on the CS_2 UV spectral concentrated in the 190–210 nm band. In 2004, Yu *et al.* constructed a gas pool with a length of 1400 m and increased the detection limit of CS_2 to 2 ppb using UV absorption spectroscopy.[16] However, studies on the quantitative detection of H_2S gas UV spectroscopy are few. The optical detection methods of H_2S are mostly photoacoustic spectroscopy and infrared spectroscopy.[12] Studies on the quantitative determination of the two mixed gases using UV differential spectroscopy are not found.

In this paper, based on the UV differential absorption spectroscopy, the optical detection platform for H_2S and CS_2 was constructed. First, the UV absorption spectra of the two gases were obtained according to the experiment. For each gas, the relationship between the absorption spectrum and the concentration was established by wavelet transform and frequency domain analysis. The cross-effects of the two kinds of gas absorption peaks at different concentrations were studied. The H_2S concentration inversion formula in the presence of CS_2 was obtained. The quantitative detection method of H_2S and CS_2 mixed gases was put forward, and the mixed gases with different mixing ratios can be detected in high accuracy. This method effectively utilizes the regularity of the absorption of two gases in the UV spectrum region, and realizes the quantitative detection of the two gases mixture, which is suitable for the quantitative detection of SF_6 decomposition components.

2 Theory

2.1 Principle of UV differential absorption spectrometry

One way of quantitatively detection by UV-DOAS is to utilize the absorption characteristics of gas molecules in the UV spectrum region. The measurement principle, based on Beer–Lambert law,[17] is as follows:

$$c = A(\lambda)/(\sigma(\lambda)L) \tag{3}$$

where, c is the concentration of the light-absorbing medium, $A(\lambda)$ is the absorbance at the corresponding wavelength position, $\sigma(\lambda)$ is the absorption cross-section, and L is the effective absorption path of the medium.

To eliminate the non-spectral noise signals, such as the dark current generated by the photodetector during the spectral acquisition process, and the background noise signal, such as the jitter of the optical fiber during the experiment, $A(\lambda)$ can be expressed as:

$$A(\lambda) = \ln\left(\frac{I'_0(\lambda) - I_N(\lambda)}{I_t(\lambda) - I_N(\lambda)}\right) \tag{4}$$

where, $I'_0(\lambda)$ is the transmitted light intensity through vessel without light-absorbing medium, $I_t(\lambda)$ is the transmitted light intensity through the light-absorbing medium, and $I_N(\lambda)$ is the dark spectrum measured when no incident light is found.

The differential absorption spectrum, as the fast-changing part, can be obtained by separating the slow-changing part from the original absorption spectrum. The fast-changing part characterizes the gas absorption spectrum information and the slow-changing part is caused by Rayleigh scattering, Mie scattering, and airflow quiver.[12] This part is defined as:

$$F(\lambda) = A(\lambda) - S(\lambda) \tag{5}$$

where,

$$S(\lambda) = \left[\sum_i c_i\sigma_{ib}(\lambda) + \varepsilon_R(\lambda) + \varepsilon_m(\lambda) + E(\lambda)\right]L \tag{6}$$

$$c' = F(\lambda)/(\sigma'(\lambda)L) \tag{7}$$

$\sigma_{ib}(\lambda)$ is the absorption cross section changing slowly with the wavelength; $\sigma'(\lambda)$ is the absorption cross section changing rapidly with the wavelength; $\varepsilon_R(\lambda)$ is the Rayleigh absorption coefficient; $E(\lambda)$ is the parameter characterizing gas jitter, instrument jitter, and other influence factors; $F(\lambda)$ is the differential absorption spectrum; and $S(\lambda)$ is the slow-changing spectrum, which can be fitted according to the basic variation of original absorbance spectrum $A(\lambda)$.

2.2 Absorption peaks of the two gases

The UV absorption spectrum of H_2S can be obtained from the MPI-Mainz database. Fig. 2 shows the UV absorption peak data of H_2S.[18–23] H_2S absorption peak is mainly concentrated in the range of 180–230 nm, which belongs to the deep UV region.

According to the CS_2 data provided by MPI-Mainz database, main absorption peaks in the UV 190–210 nm band and weak absorption peaks in the 285–340 nm band are found.[24–29] As it's shown in Fig. 3.

Therefore, due to the spectra superimposed in the wavenumber domain, H_2S cannot be quantitatively analyzed by using the concentration inversion expression of single gas directly. However, given that CS_2 is not affected in the wavenumber domain by H_2S, CS_2 can be quantified by the inversion formula of CS_2. Therefore, if we can find the influence rule of CS_2 on H_2S, then the H_2S quantification in the mixed gases can be realized. This finding is also the key to achieving simultaneous detection for mixing gas of CS_2 and H_2S.

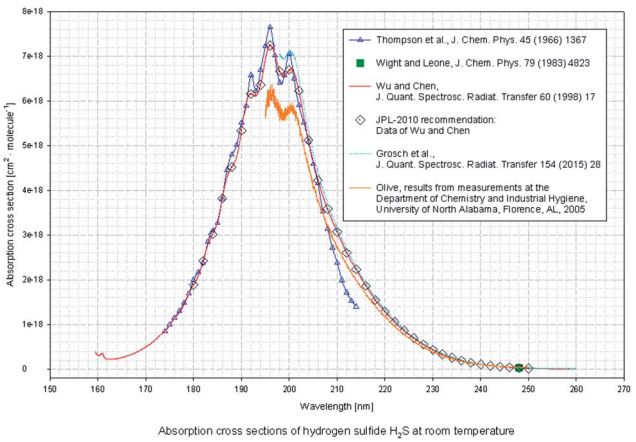

Fig. 2 UV absorption cross section spectra of H_2S.

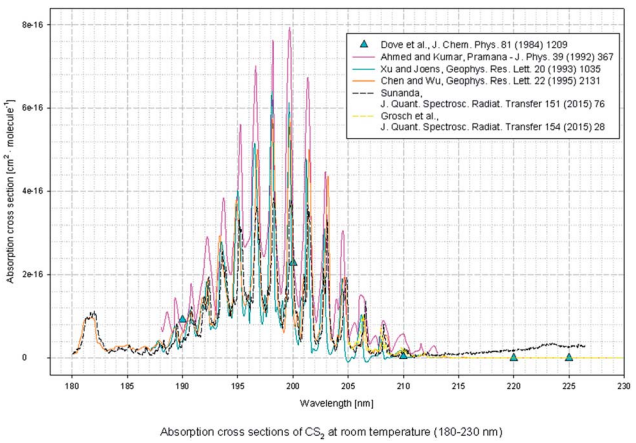

Fig. 3 UV absorption cross section spectra of CS_2.

3 Experiment

3.1 Experiment set

This platform mainly includes UV light source, gas absorption cell, spectrometer, host computer, gas sample compounder, vacuum pump, and other components, shown in Fig. 4. Among them, the UV light source (Ocean Optics D2000) can output 190–400 nm range of stable UV spectrum, a peak-to-peak stability of less than 0.005%, and per hour drift is within 0.5%. With regard the spectrometer (Ocean Optics maya2000pro spectrometer), the spectral range of 165–1100 nm, and the standard optical resolution is at 0.25 nm. Fibers (Ocean Optics QP600) can achieve 80% transmittance above 180 nm. The gas absorption cell is made of custom stainless steel. The internal light is reflected once, and the optical path length is 0.8 m. The inner wall of the cell is coated with Teflon coating, which can effectively prevent the adsorption of test gases. The gas distributor is a gas sample compounder, which has the largest dilution ratio is of 300 : 1 and an accuracy of ±1% FS. Standard gases (Newradargas Co., Ltd., Wuhan) are high purity nitrogen, 2 ppm CS_2, and 50 ppm H_2S.

3.2 Experimental operation

We prepared different concentrations for the two kinds of single gas and the different ratios of mixed gases by gas sample compounder. The specific mix ratio is discussed in Section 3.3. The experimental gases were prepared from low to high concentration. Before the test, the gas cell was cleaned three to five times with high-purity nitrogen gas. Each time, the cell was vacuumed and inflated to atmospheric pressure with nitrogen, then left to stand for 3 min. After cleaning, the cell was inflated to atmospheric pressure with nitrogen. The dark spectrum is collected in the case of no-light, and the background spectrum

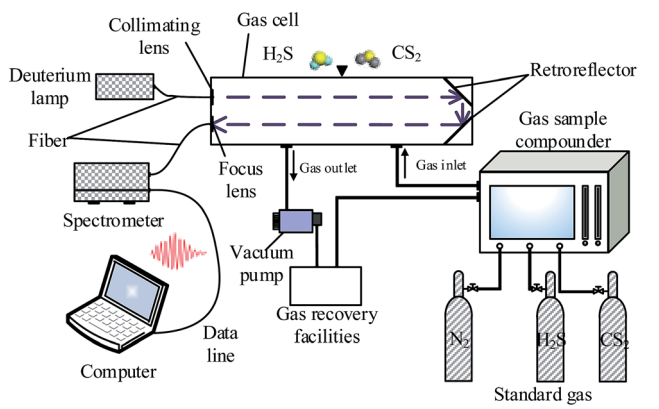

Fig. 4 Schematic diagram of the UV-DOAS detection system.

Table 1 Mixture gases of CS_2 and H_2S

	H_2S (ppm)				
CS_2 (ppb)	1	2	5	10	20
10		✓		✓	
20	✓		✓		✓
50		✓		✓	
100	✓		✓		✓
200		✓		✓	

is collected in the case of with-UV-light, and the light source is confirmed to be stable by the spectrometer before collecting the background spectrum. Finally, the test gases are collected in a low-to-high-concentration order. The gas cell was evacuated and washed twice after each detection. Each group was collected with 10 spectral data; one of which was used for quantitative analysis, and the other nine groups were used to verify the concentration inversion expression. The obtained dark spectrum, the background spectrum, and the test gas spectrum were placed into the formula (4) to calculate UV absorption spectrum. Through the baseline deduction to remove the slow-changing part of the spectrum, differential optical absorption spectrum can be obtained as described in formula (5).

3.3 Filters of the spectrum

The UV differential absorption spectra directly obtained by experiments cannot obtain good detection accuracy. On the one hand, the existence of some noise that cannot be removed by UV-DOAS theory. On the other hand, the measurement of mixed gases will cause the spectrum to superimpose, which is not enough to achieve the effective separation of the two gas spectra in the wavelength domain; this finding means that quantitative detection of mixing components cannot be achieved. To solve the above problems, this paper combined the wavelet transform and FFT transform to extract further the feature quantity in the UV differential absorption spectrum and to eliminate the effect of the interference noise. In this paper, Meyer wavelet is used. The wavelet function and this wavelet's scale function are both defined in the frequency domain and have a fast convergence rate. Through the experimental test, the optimal wavelet scale for CS_2 and H_2S filtering is 10 and 33, respectively. Interference noise in the spectrum was removed by Meyer wavelet filter, and the feature information is enhanced several times. The details are discussed in Section 4.1.

3.4 Gas distribution

Compared with CS_2, H_2S are more likely to produce and with a produce higher yield in POF fault,[30,31] so go to the following concentration. For each single gas, H_2S test gas was prepared in 1, 2, 5, 10, and 20 ppm, CS_2 test gas were prepared in 10, 20, 50, 100 and 200 ppb. The mixtures of both gases prepared in nitrogen because SF_6 and N_2 neither has absorption in 190–400 nm and don't have a interference for detection.

The mixing gas for the two gases is shown in Table 1, where, "✓" indicates that the combination is prepared.

The gas distribution process can be described as follows: (a) CS_2 was kept constant at 20 or 100 ppb, and we adjusted the H_2S at 1, 5, and 20 ppm from low to high concentration at each CS_2 concentration. (b) H_2S was kept at 2 or 10 ppm unchanged, adjusting the CS_2 at 10, 50, and 200 ppb in turn from low to high concentrations at each H_2S concentration.

4 Results and discussion

4.1 Single-gas inversion expression

4.1.1 H_2S. Through a large number of experiments, the results are shown in Fig. 5. Fig. 5(a) shows the UV absorption spectra of H_2S at different concentrations. The overall absorbance increases with the increase of the concentration. UV absorption of H_2S ranges from 190 nm to 250 nm; however, the narrow band absorption is only around 190–210 nm.

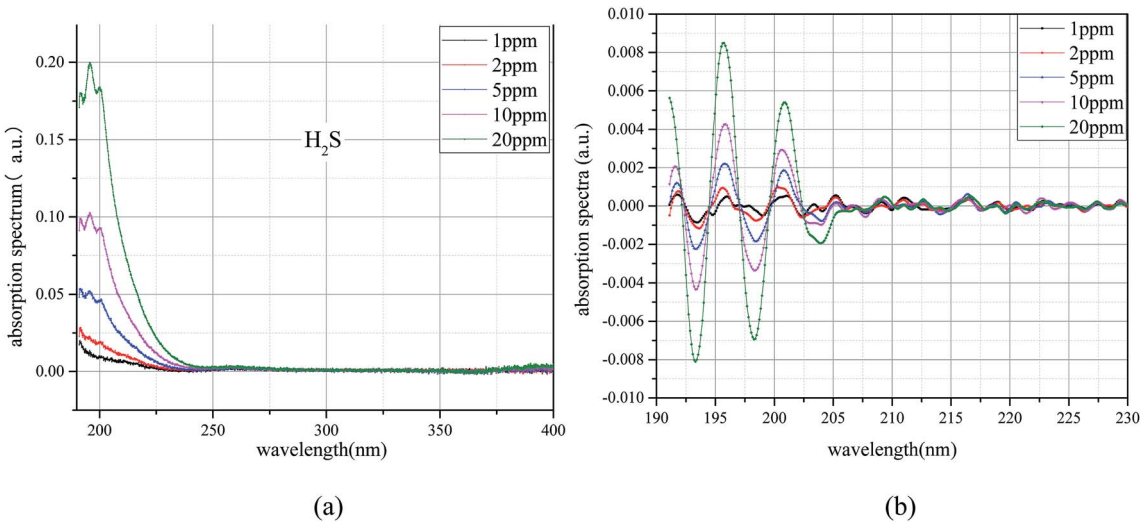

Fig. 5 UV spectrum of H_2S. (a) UV absorption spectrum. (b) Differential spectrum.

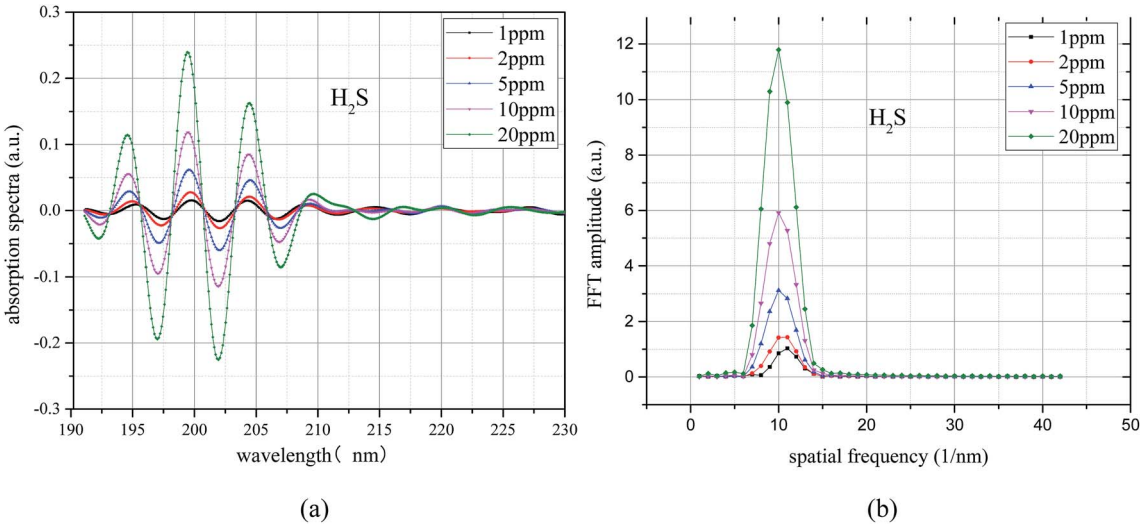

Fig. 6 H_2S differential absorption spectroscopy after filtering and its FFT spectrum. (a) Differential spectrum after filter. (b) FFT frequency spectrogram.

Concentration of H_2S of 5, 10, and 20 ppm showed a narrow band absorption, whereas the narrow band absorption is very weak for 2 and 1 ppm H_2S. Fig. 5(b) is the corresponding UV difference absorption spectra extracted from the UV absorption spectra of H_2S at different concentrations. Data are not found with regard the absorption in the rear band of 210 nm, and the H_2S at each concentration shows narrowband absorption. The narrowband absorption of H_2S gradually increases with the increase of the concentration. The UV differential absorption spectra of H_2S are affected by the high-frequency noise; the lower the concentration, the more serious the influence there is.

A bandpass filter algorithm for the extraction of UV differential absorption spectra of H_2S was constructed by using Meyer wavelet. The differential absorption spectrum after treatment is shown in Fig. 6(a), and the UV absorption spectrum after filtering is further transformed by FFT; the results shown in Fig. 6(b). Fig. 6(a) shows that (1) the characteristic information of the UV differential absorption spectrum is very concentrated, almost no high and low wave number of noise interference, (2) peaks of different concentrations appear at the same position ($10\ nm^{-1}$), and the peak value of H_2S increases with the increase of H_2S concentration; this finding means that the concentration can be well characterized.

To avoid the randomness of single data point, the algebraic sum of the FFT values of three points ($9\ nm^{-1}$, 10, and $11\ nm^{-1}$) is chosen as the FFT eigenvalues to characterize the trace H_2S concentration. The FFT eigenvalues at different concentrations were calculated. Least squares method was used to linearly fit the H_2S concentration and its corresponding FFT eigenvalues. The fitting results are shown in Fig. 7. The FFT eigenvalues and H_2S concentration have a high degree of linearity, which reaches 0.9999 (R^2). H_2S concentration can be obtained by inversion expression as:

$$y = 1.564x + 0.571 \quad (8)$$

where, y is the FFT eigenvalue of the H_2S, and x is the H_2S concentration (ppm). The uncertainty of slope and intercept is 4.83×10^{-3} and 4.98×10^{-2}.

4.1.2 CS_2. The obtained CS_2 UV absorption spectrum at each concentration is shown in Fig. 8(a). CS_2 has UV absorption at each concentration, and the absorption is increased with the increase of concentration. The interval between the narrow band absorption peaks is significantly smaller than that of H_2S. The UV differential absorption spectra at each concentration were extracted, and the results are shown in Fig. 8(b). The UV differential absorption spectra of CS_2 at different concentrations show similar characteristics. With the increase of the concentration, the differential absorption is enhanced. When

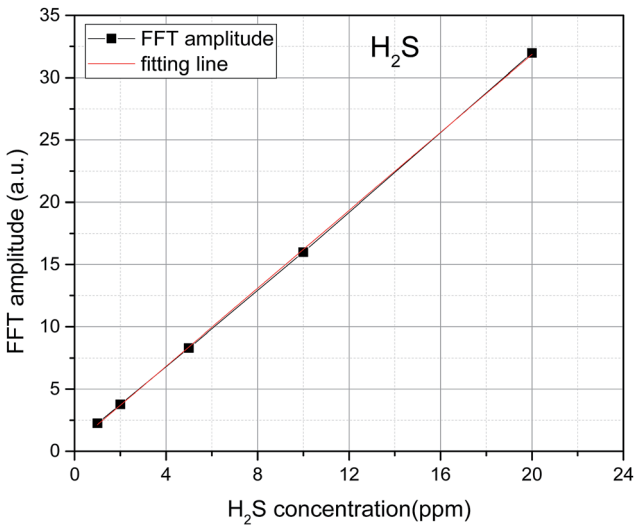

Fig. 7 Relationship between FFT eigenvalue and H_2S concentration.

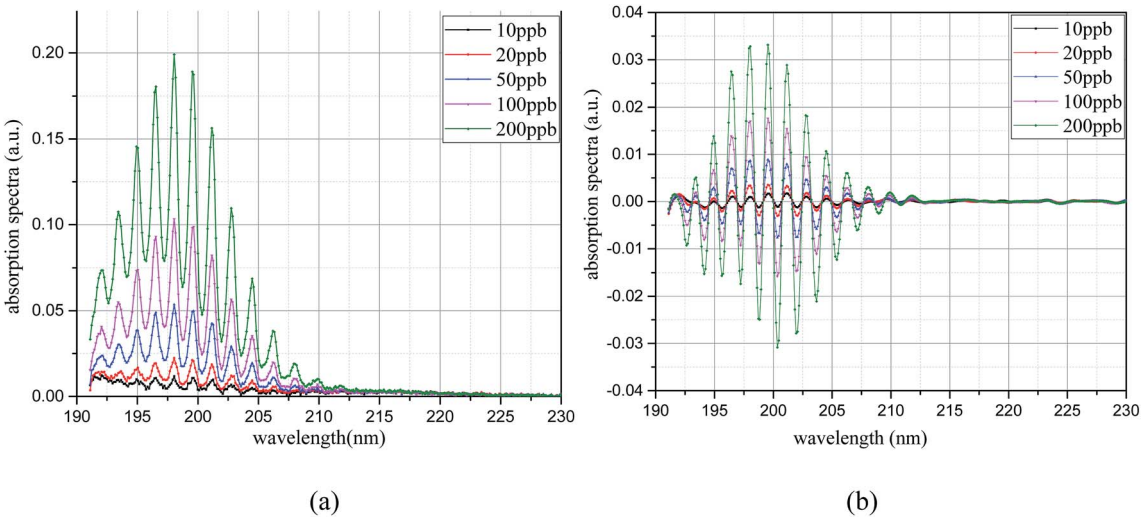

(a) (b)

Fig. 8 UV spectrum of CS_2. (a) UV absorption spectrum. (b) Differential spectrum.

the CS_2 concentration is low, high-frequency noise in the differential spectrum is observed, and the spectrum is easily affected.

The UV differential absorption spectra of each CS_2 concentration were filtered using the Meyer wavelet; the results are shown in Fig. 9(a). In the figure, the differential absorption spectra of each concentration after filtering treatment are more obvious and the spectrum is very smooth. Almost no interference information is found. With the increase of concentration, the spectral characteristics of CS_2 are similar, and the absorption gradually strengthens. The FFT frequency spectrogram results are shown in Fig. 9(b). Fig. 9(b) shows that the characteristic information is concentrated after filtering treatment, and the peak appears at 30 nm^{-1}, which is different from H_2S. With the increase of CS_2 concentration, the FFT value increases simultaneously. Therefore, the UV differential absorption spectrum after filtering and its FFT value in the wavenumber domain have the ability to realize quantitative analysis of CS_2. The FFT eigenvalues of the UV absorption spectrum were used for CS_2 concentration inversion.

The algebraic sum of the FFT values (9, 30, and 31 nm^{-1}) is chosen as the FFT eigenvalues to characterize the concentration of CS_2, and the least squares method is used to linearly fit the concentration and FFT eigenvalues. In Fig. 10, results show a high degree of linear relationship between the FFT eigenvalues and CS_2 concentration, and the linearity (R^2) is as high as 0.9998. The inversion expression is:

$$y = 0.1434x + 0.1062 \quad (9)$$

where, y represents the FFT eigenvalue of the CS_2, and x represents the CS_2 concentration in ppb. The uncertainty of slope and intercept is 7.58×10^{-4} and 7.76×10^{-2}.

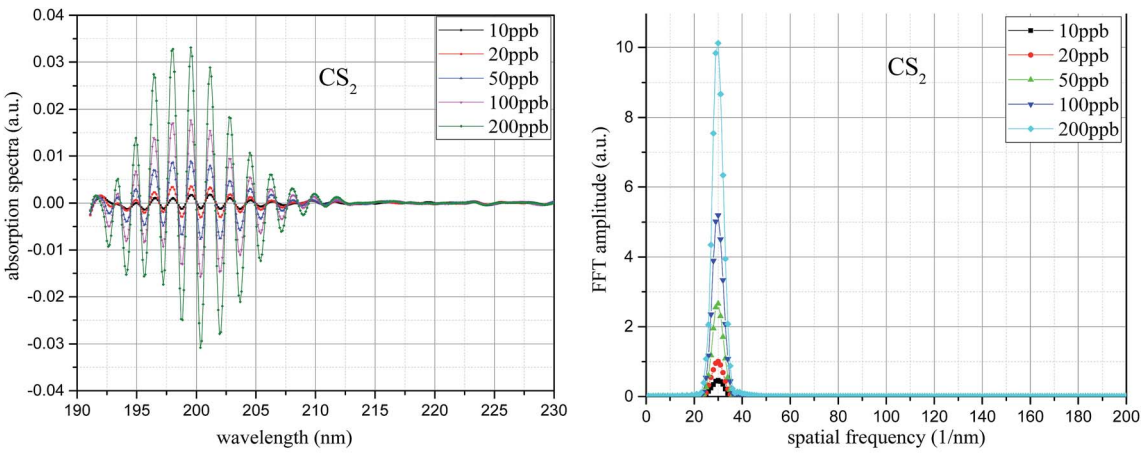

(a) (b)

Fig. 9 UV difference absorption spectroscopy after filtering and its FFT spectrum. (a) Differential spectrum after filter. (b) FFT frequency spectrogram.

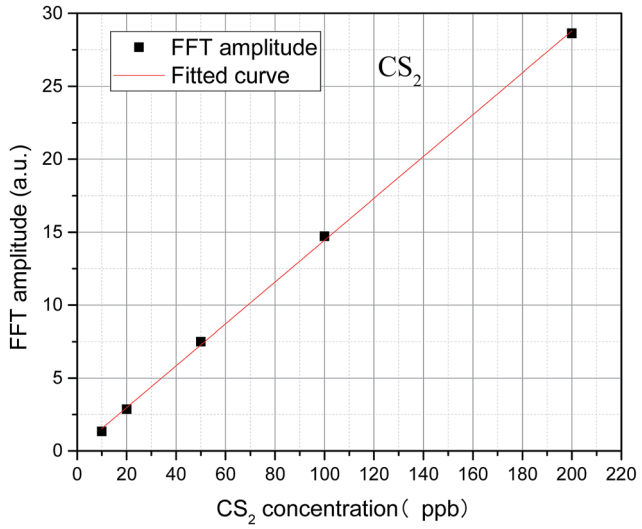

Fig. 10 Relationship between FFT eigenvalue and CS_2 concentration.

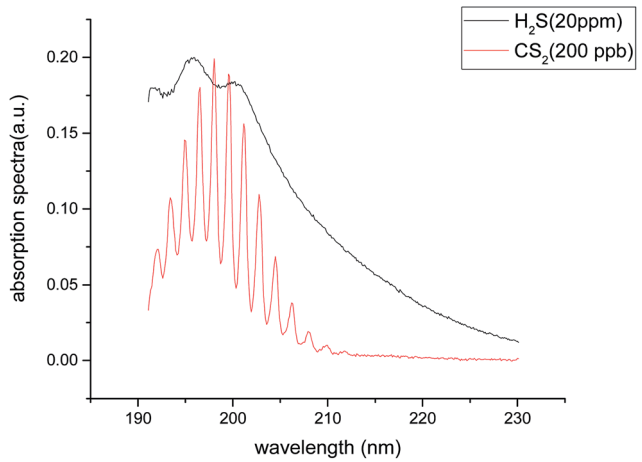

Fig. 11 The superposition of the two respectively UV absorption spectra of two gases.

4.2 Mixed gas detection

In Fig. 1 and 2, the absorption coefficient of CS_2 is about two orders of magnitude larger than that of H_2S. To visually show the intersection of the two kinds of gases near UV 200 nm band, the spectra of 20 part per million (ppm) of H_2S and 200 part per billion (ppb) of CS_2 are detected, and the two are superimposed on Fig. 3.

In Fig. 11, the two gases in the UV spectrum region have a serious cross; this finding means that each absorption spectra of the two gases cannot be separated directly by UV differential spectroscopy, and the two gas concentrations cannot be obtained by inversion method. The slow-changing part of the absorption spectrum was removed by baseline deduction, and the differential absorption spectrum was obtained. The obtained differential spectrum was inverted into the frequency domain by FFT transform. The results are shown in Fig. 12.

Fig. 12 shows that the differential absorption spectra of the two gases are superimposed in the wavelength domain, and the UV differential absorption spectra of H_2S are all submerged in the spectra of CS_2. Fig. 4(b) shows that the eigenvalues of CS_2 in wavenumber domain are not affected by H_2S; however, the CS_2 contains characteristic information for H_2S quantification, which will have an effect on the quantitative detection of H_2S.

4.2.1 Inversion results. The mixed gases are prepared as discussed in Section 3.4. The spectral data of each mixture were collected in 10 groups to avoid experimental errors. The differential absorption spectra of the two gases were extracted by the filters, and the CS_2 and H_2S concentrations were calculated by using the concentration inversion expressions in Section 4.1. The results are shown in Table 2. The concentrations were calculated by taking the average after the minimum and maximum were removed in 1 of the 10 groups. Δ_h is the difference value between the calculation results and the actual concentration of H_2S. δ is the percentage of error. In Table 2, the relationship between the inversion concentration and the actual concentration of the two gases were described.

In Fig. 13, the linearity (R^2) of CS_2 concentration is up to 0.9997 mixed with different H_2S concentrations; this result indicates that the presence of mixed H_2S has little effect on CS_2 concentration inversion. In Table 2 and Fig. 14, when the CS_2

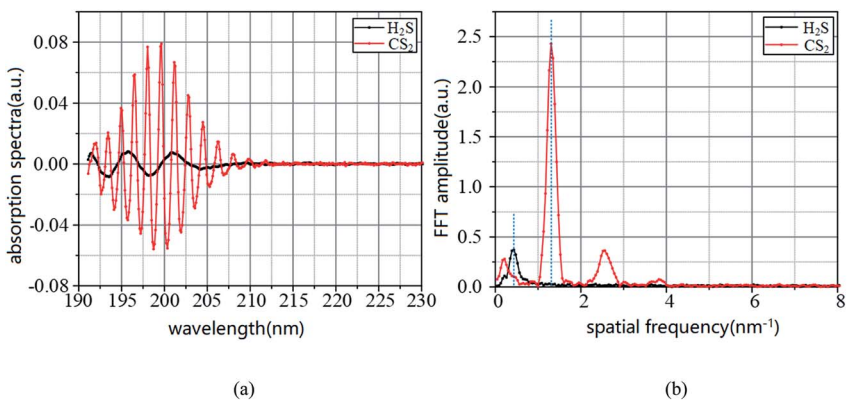

Fig. 12 UV difference absorption spectra of CS_2 and H_2S and its FFT spectra. (a) Differential spectrum. (b) FFT frequency spectrogram.

Table 2 Direct inversion results of CS_2 and H_2S mixed gases

CS_2 (ppb)		Inversion concentration			Δ_h (ppm)	δ (%)
20		19.7	19.9	19.0		
H_2S (ppm)	1	0.96			−0.04	4
	5	4.95			−0.05	1
	20	20.19			0.19	0.95

CS_2 (ppb)		Inversion concentration			Δ_h (ppm)	Δ (%)
100		99.8	101.3	99.01		
H_2S (ppm)	1	3.03			2.03	203
	5	6.91			1.91	38.2
	20	21.85			1.85	9.25

H_2S (ppm)		Inversion concentration			Δ_h (ppb)	δ (%)
2		1.99	2.58	6.57		
CS_2 (ppb)	10	8.9			−0.01	0.1
	50	51.4			0.58	1.16
	200	196.5			4.57	2.23

H_2S (ppm)		Inversion concentration			Δ_h (ppb)	Δ (%)
10		10.23	10.56	14.10		
CS_2 (ppb)	10	9.5			0.23	2.3
	50	51.4			0.56	1.12
	200	197.1			4.10	2.05

concentration is small (10 and 20 ppb), little effect on the inversion of H_2S is observed. However, when the concentration of CS_2 is large (50, 100, and 200 ppb), the inversion of H_2S concentration is disturbed. Besides, the effect basically shows a linear increase with the increase of CS_2 concentration. The two fitting lines shown in Fig. 14 are almost parallel; this result indicates that the same concentration of CS_2 has a relatively close effect on different concentrations of H_2S. Thus, the lower concentration of H_2S is disturbed more by CS_2.

4.2.2 Correction expression of H_2S. In accordance to the previous section, the concentration of CS_2 in the mixed gases of H_2S and CS_2 can be calculated directly, and the H_2S concentration inversion expression must be corrected. Considering the H_2S detection limit, and the unavoidable errors, such as gas operation. Low concentration detection should be of priority. The concentration effects were calculated through the three concentrations. CS_2 in 50, 100, and 200 ppb were set to 0.6, 2.0, and 4.6 ppm H_2S increase. The correction expression was

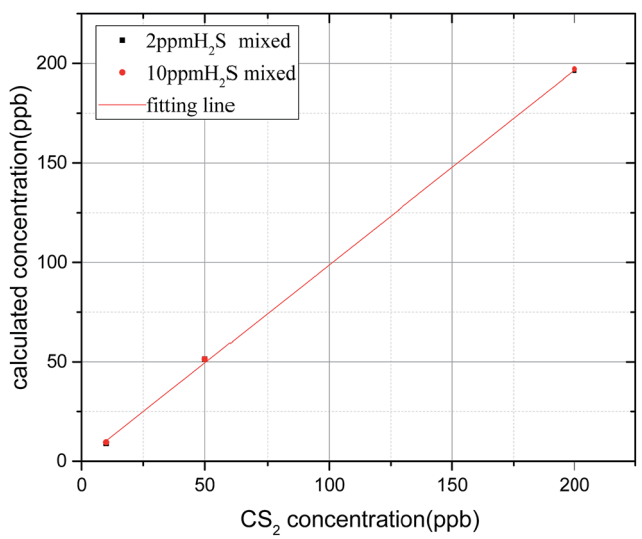

Fig. 13 Inversion concentration of CS_2 with different concentrations of H_2S.

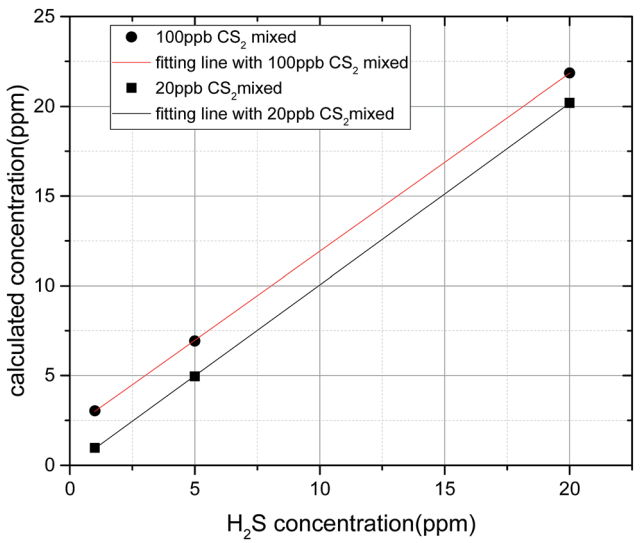

Fig. 14 Inversion concentration of H_2S with different concentrations of CS_2.

Table 3 Revised inversion results of H_2S in mixed gases

(a)			(b)			(c)		
20 ppb CS_2			50 ppb CS_2			150 ppb CS_2		
c_H	c_h	Δ_h	c_H	c_h	Δ_h	c_H	c_h	Δ_h
1	0.65	−0.35	1	0.97	0.03	1	1.12	0.12
2	1.82	0.18	2	1.99	0.01	2	1.67	−0.33
5	5.04	0.04	5	5.15	0.15	5	4.50	0.50
10	10.29	0.29	10	10.27	0.27	10	10.03	0.03
15	15.27	0.27	15	15.20	0.20	15	14.85	−0.15
20	20.27	0.27	20	19.80	−0.2	20	19.81	−0.19

determined based on the determined influence value, shown as formula (10).

$$\Delta_h = 0.0259 \times c_c - 0.45 \ (R^2 = 0.9997) \quad (10)$$

where, Δ_h represents the increase in H_2S caused by CS_2 (unit: ppm). c_c represents the concentration of CS_2 (unit: ppb).

4.2.3 Inversion with correction expression. We changed a set of gas concentration to check the correction expression. The concentration of H_2S in mixed gases was detected and calculated again; results are shown in Table 3 c_H is the actual concentration of H_2S. c_h is the inversion result. Δ_h is the difference value between c_H and c_h, in ppm. The results show the effect of the correction expression, and the inversion values can nearly reflect the actual concentration.

In Fig. 15, the corrected straight line has a high linearity, and the concentration inversion of H_2S is very accurate. The linearity (R^2) is 0.9994, which means that the correction expression can be used in the detection of the two gas mixture.

Therefore, for the quantitative detection of H_2S and CS_2 mixed gases, the concentration of H_2S and CS_2 can be calculated by the expressions (8) and (9) after the differential spectrum was obtained. Then, H_2S was corrected with expression (10) to obtain accurate concentration.

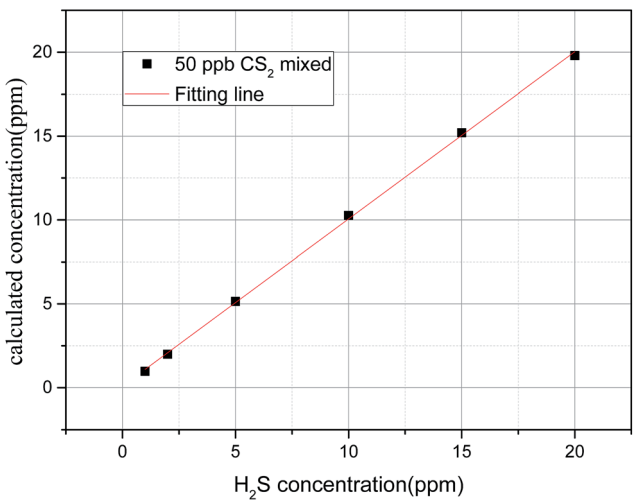

Fig. 15 Fitting straight line of H_2S after correction.

5 Conclusion

In this paper, the detection platform of H_2S and CS_2 based on UV absorption spectroscopy was established. First, two kinds of single gases were detected, and the concentration inversion expressions of the two gases were obtained. After that, the mixed gases at different ratios were detected. H_2S has little effect on the detection of CS_2, and the effect of CS_2 on H_2S concentration inversion is linear with CS_2 concentration. Basing on the data analysis, we obtained the correction expression of CS_2 gas to H_2S concentration. Expression validity was proved by the actual data verification. Hence, the H_2S and CS_2 gas can be detected by using the proposed modified detection expressions, which can realize the high-precision quantitative detection of the two gases and provide technical support for the online monitoring of SF_6 decomposition components.

Conflicts of interest

There are no conflicts to declare.

References

1 L. G. Christophorou and J. K. Olthoff, Electron Interactions with SF6, *IEEE International Conference on Plasma Science, 1996. IEEE Conference Record*, IEEE, 1999, p. 107.
2 F. Y. Chu, SF6 Decomposition in Gas-Insulated Equipment, *IEEE Trans. Electr. Insul.*, 1986, **EI-21**(5), 693–725.
3 J. Tang, F. Zeng, J. Pan, *et al.*, Correlation analysis between formation process of SF6, decomposed components and partial discharge qualities, *IEEE Trans. Dielectr. Electr. Insul.*, 2013, **20**(3), 864–875.
4 X. Zhang, J. Zhang, Y. Jia, *et al.*, TiO2 Nanotube Array Sensor for Detecting the SF6 Decomposition Product SO2, *Sensors*, 2012, **12**(3), 3302–3313.
5 S. Pokharel, Spatial analysis of rural energy system, *Int. J. Geogr. Inform. Sci.*, 2000, **14**(8), 855–873.
6 F. Zeng, J. Tang, Y. Xie, *et al.*, Experimence Study of Trace Water and Oxygen Impact on SF6 Decomposition Characteristics Under Partial Discharge, *Journal of Electrical Engineering & Technology*, 2015, **10**(4), 1787–1796.
7 X. Zhang, H. Zhou, C. Chen, *et al.*, Ultraviolet Differential Optical Absorption Spectrometry: Quantitative Analysis of the CS2 Produced by SF6 Decomposition, *Meas. Sci. Technol.*, 2017, **28**, 115102.
8 M. Mortimer and P. G. Taylor, *Chemical kinetics and reaction mechanism*, Springer Verlag, Berlin, Germany, 2002.
9 X. Zhang, L. Yu, Y. Gui, *et al.*, First-principles study of SF6, decomposed gas adsorbed on Au-decorated graphene, *Appl. Surf. Sci.*, 2016, **367**, 259–269.
10 F. Y. Chu, SF6 decomposition in gas-insulated equipment, *IEEE Trans. Electr. Insul.*, 1986, (5), 693–725.
11 X. Zhang, H. Liu, J. Ren, *et al.*, Fourier transform infrared spectroscopy quantitative analysis of SF 6 partial discharge decomposition components, *Spectrochim. Acta, Part A*, 2015, **136**, 884–889.

12 X. Zhang, Z. Cheng and X. Li, Cantilever Enhanced Photoacoustic Spectrometry: Quantitative Analysis of the Trace H2S produced by SF6 Decomposition, *Infrared Phys. Technol.*, 2016, **78**, 31–39.

13 X. Cui, C. Lengignon, W. Tao, *et al.*, Photonic sensing of the atmosphere by absorption spectroscopy, *J. Quant. Spectrosc. Radiat. Transfer*, 2012, **113**(11), 1300–1316.

14 M. Wenig, B. Jähne and U. Platt, Operator representation as a new differential optical absorption spectroscopy formalism, *Appl. Opt.*, 2005, **44**(16), 3246–3253.

15 J. Mellqvist and A. Rosén, DOAS for flue gas monitoring—I. Temperature effects in the UV/visible absorption spectra of NO, NO2, SO2 and NH3, *J. Quant. Spectrosc. Radiat. Transfer*, 1996, **56**(2), 187–208.

16 Y. Yu, A. Geyer, P. Xie, B. Galle, L. Chen and U. Platt, Observations of carbon disulfide by differential optical absorption spectroscopy in Shanghai, *Geophys. Res. Lett.*, 2004, **31**, L11107.

17 L. Wang, Y. Zhang, X. Zhou, *et al.*, Optical sulfur dioxide sensor based on broadband absorption spectroscopy in the wavelength range of 198–222 nm, *Sens. Actuators, B*, 2017, **241**, 146–150.

18 S. D. Thompson, D. G. Carroll, F. Watson, *et al.*, Electronic Spectra and Structure of Sulfur Compounds, *J. Chem. Phys.*, 1966, **45**(5), 1367–1379.

19 C. A. Wight and S. R. Leone, Vibrational state distributions and absolute excitation efficiencies for T-V transfer collisions of NO and CO with H atoms produced by excimer laser photolysis, *J. Chem. Phys.*, 1983, **79**(10), 4823–4829.

20 C. Y. R. Wu and F. Z. Chen, Temperature-dependent photoabsorption cross sections of H2S in the 1600–2600 Å region, *J. Quant. Spectrosc. Radiat. Transfer*, 1999, **61**(2), 265–271.

21 L. Chen, J. Wu and R. Jia, *et al.*, Recommendation on Uncertain Services, *IEEE International Conference on Web Services*, IEEE Computer Society, 2010, pp. 683–684.

22 H. Grosch, A. Fateev and S. Clausen, UV absorption cross-sections of selected sulfur-containing compounds at temperatures up to 500 °C, *J. Quant. Spectrosc. Radiat. Transfer*, 2015, **154**, 28–34.

23 B. Olive, *Result from measurements at the department of chemistry and industrial hygiene*, University of North Alabama, Florence, al, 2005.

24 J. E. Dove, H. Hippler, H. J. Plach, *et al.*, Ultraviolet spectra of vibrationally highly excited CS2 molecules, *J. Chem. Phys.*, 1984, **81**(3), 1209–1214.

25 S. M. Ahmed and V. Kumar, Measurement of photoabsorption and fluorescence cross-sections for CS 2, at 188.2–213 and 287.5–339.5 nm, *Pramana*, 1992, **39**(4), 367–380.

26 H. Xu and J. A. Joens, CS2 absorption cross-section measurements from 187 nm to 230 nm, *Geophys. Res. Lett.*, 1993, **20**(11), 1035–1037.

27 F. Z. Chen and C. Y. R. Wu, High, room and low temperature photoabsorption cross sections of CS2 in the 1800–2300 Å region, *Geophys. Res. Lett.*, 1995, **22**(16), 2131–2134.

28 S. K. Kumar, A. Shastri, A. K. Das and B. N. Raja Sekhar, Electronic states of carbon disulphide in the 5.5–11.8 eV region by VUV photo absorption spectroscopy, *J. Quant. Spectrosc. Radiat. Transfer*, 2015, **151**, 76–87.

29 H. Grosch, A. Fateev and S. Clausen, UV absorption cross-sections of selected sulfur-containing compounds at temperatures up to 500 °C, *J. Quant. Spectrosc. Radiat. Transfer*, 2015, **154**, 28–34.

30 L. Cheng, J. Tang and X. Huang, *et al.*, SF6 partial overheating decomposition characteristics with organic insulating materials, *Gaodianya Jishu/high Voltage Engineering*, 2015, vol. 41(2), pp. 453–460.

31 F. Zeng, *et al.*, Decomposition characteristics of SF6 under thermal fault for temperatures below 400 °C, *IEEE Trans. Dielectr. Electr. Insul.*, 2014, **21**(3), 995–1004.

